

Calculation of Transonic Steady and Oscillatory Pressures on a Low Aspect Ratio Model

Robert M. Bennett* and Eleanor C. Wynne†
NASA Langley Research Center, Hampton, Virginia

and
 Dennis G. Mabey‡
RAE Dynamics Laboratory, Bedford, England

Pressure data measured by the British Royal Aircraft Establishment for the AGARD SMP tailplane are compared with results calculated using the transonic small perturbation code XTRAN3S. A brief description of the analysis is given and a recently developed finite-difference grid is described. Results are presented for four steady and eight harmonically oscillating cases near zero angle of attack and for a range of subsonic and transonic Mach numbers.

Nomenclature

c	= airfoil chord, m
C_p	= pressure coefficient
C_p^*	= critical pressure coefficient
\bar{C}_p	= normalized unsteady pressure coefficient; first harmonic of C_p divided by oscillation amplitude in radians
c_r	= wing reference chord, m
f	= oscillation frequency, Hz
k	= reduced frequency, $\omega c_r / 2V$
M	= freestream Mach number
r	= function defining instantaneous position of wing surface, $z = r(x, y, t)$
t	= time, s
V	= freestream velocity, m/s
x, y, z	= coordinates of a right-hand Cartesian system with origin at wing root leading edge, positive x in downstream direction, y in spanwise direction, and z up, m
α	= wing angle of attack, deg
γ	= ratio of specific heats
η	= fraction of semispan
ξ, η, ζ	= transformed coordinates in x, y , and z directions, respectively
ϕ	= perturbation velocity potential
τ	= transformed time, $\tau = t$
ω	= angular frequency, $2\pi f$, rad/s

Introduction

THE transonic speed range is a critical region for many aeroelastic phenomena, such as flutter and divergence. In the past, analytical methods have been unable to accurately model the nonlinear transonic aerodynamics, and analysts have used linear theory for estimates of transonic aeroelastic behavior. Reliance was placed primarily on tests of scaled aeroelastic models and flight tests of the aircraft for flutter clearance and aeroelastic deformation effects. Recently, considerable progress has been made in calculating steady tran-

sonic flows about aircraft using finite-difference methods to obtain numerical solutions of the flow equations. Significant progress is also being made toward developing finite-difference methods for unsteady flows which may eventually lead to accurate transonic aeroelastic analyses.

For two-dimensional flows, methods based on the transonic small perturbation (TSP) equation have been developed and extensively applied (see Refs. 1 and 2, for example). These methods have been extended to include viscous effects,^{3,4} nonisentropic effects,⁵ and wing-canard configurations.⁶ For three-dimensional flows, the XTRAN3S program has been developed⁷ by the Boeing Company under USAF contract. It is also based on the isentropic TSP equation and treats an isolated planar wing including aeroelastic deformation effects and unsteady motion. The XTRAN3S program has been implemented on the Control Data Corporation VPS32 computer at the NASA Langley Research Center. A variety of applications are being made in order to evaluate its applicability to several types of wings.

Several organizations have expended significant effort to measure static and oscillatory pressures on wings at transonic speeds for use in evaluating the computational methods and to improve the understanding of unsteady transonic flows. For example, configurations tested at the Langley Research Center include a clipped delta wing with a 6% thick circular arc airfoil section,⁸ an advanced transport wing with several oscillating controls,⁹ an oscillating rectangular wing with a supercritical airfoil,¹⁰ and a flexible supercritical wing from the DAST ARW-2 vehicle.¹¹ Pressures for several of these have been calculated using XTRAN3S.^{12,13} Calculations have also been made^{14,15} for the F-5 and LANN wings¹⁶ which were tested at NLR.^{16,17} The British Royal Aircraft Establishment (RAE) has recently measured oscillating and static pressures on a model called the AGARD SMP tailplane model.¹⁸ This configuration is sufficiently different from the others that it supplements them for verifying transonic codes. Comparison of some of these experimental results with calculations made using the XTRAN3S code is the subject of this report.

In this paper, a brief description of the tailplane model and the test program is presented first. Next the XTRAN3S program and a recently improved finite-difference grid and coordinate transformation are described. Finally, comparisons of calculated and measured steady and unsteady pressures for several subsonic and transonic Mach numbers are presented and discussed.

It should be noted that the unsteady experimental data presented in the original paper were in error for the outboard three chords of the wing. The errors occurred in the plotting of the experimental data and have been corrected for the results

Received July 24, 1985; revision received Nov. 19, 1986. Copyright © 1987 American Institute of Aeronautics and Astronautics, Inc. No copyright is asserted in the United States under Title 17, U.S. Code. The U.S. Government has a royalty-free license to exercise all rights under the copyright claimed herein for Governmental purposes. All other rights are reserved by the copyright owner.

*Sr. Research Engineer, Unsteady Aerodynamics Branch, Member AIAA.

†Mathematical/Data Analysis, Unsteady Aerodynamics Branch.

‡Principal Scientific Officer, Aerodynamics Department.

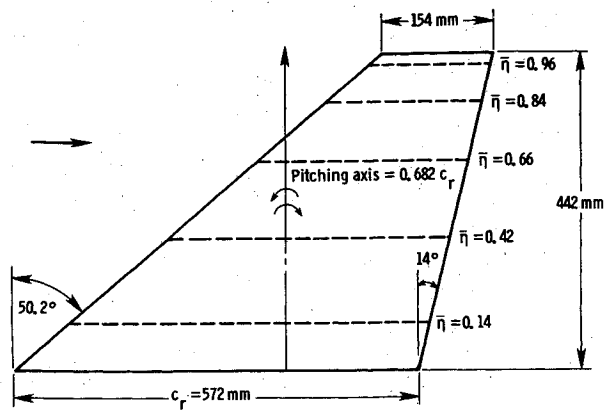


Fig. 1 Planform of AGARD SMP tailplane model.

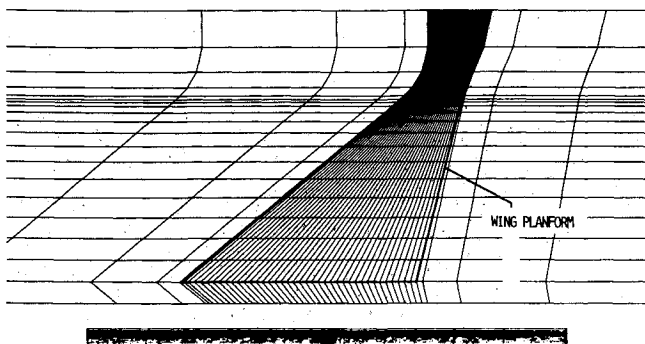
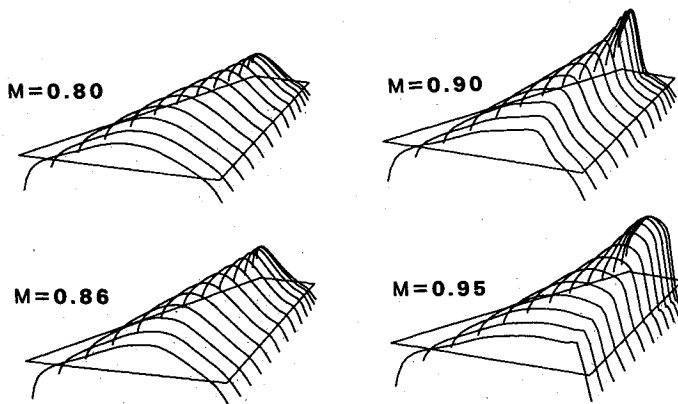


Fig. 2 Finite-difference grid in the plane of the wing and near- and far-field views.

Fig. 3 Calculated upper surface distribution ($-C_p$) for several Mach numbers, $\alpha = -0.3$ deg.

presented in Figs. 5 and 6 herein. The steady data and the two inboard chords were unaffected.

Description of RAE AGARD Tailplane and Test

The planform of the RAE tailplane model¹⁸ is shown in Fig. 1. The model was molded from graphite fiber and has a full span aspect ratio of 2.41, a taper ratio of 0.27, and a leading edge sweep angle of 50.2 deg. The root chord, c_r , is 0.572 m (1.88 ft) and the span is 0.442 m (1.45 ft or 0.773 c_r). The airfoil is approximately a symmetric NACA 64A010.2, and

measured ordinates for the model were used in the present calculations. A hydraulic drive mechanism was used to oscillate the model in pitch about an axis at 68.2% of the root chord with an amplitude of approximately 0.4 deg. The oscillation frequencies were 3, 12, 33, and 70 Hz, and the model was oscillated about steady angles of attack of up to ± 5 deg. Only the dynamic data for angles of attack near 0 deg and for frequencies of 33 and 70 Hz are used herein.

Pressures were measured along five span stations (Fig. 1) with 20 pressure transducers located along the upper surface of the wing at each span station. The same pressure gages were used both for the steady and unsteady measurements. The data acquisition system restricted simultaneous measurements to only two chords. The data give the static pressures, and the mean, magnitude, and phase of the oscillating pressures. The tests were conducted in the RAE 3-ft wind tunnel at RAE Bedford and were run for Mach numbers ranging from 0.65–1.20 in the slotted transonic test section, and for Mach numbers 1.32–1.72 in the closed supersonic section. Tests were performed at constant pressure, and the Reynolds number at a Mach number of 0.86 was 3 million based on the wing semispan. Transition strips were also placed on the model at 0.075 chord. A more complete description of the model and tests is given in Ref. 18.

XTRAN3S Program Description

The modified unsteady small perturbation (TSP) potential equation that is solved by XTRAN3S⁷ is

$$M^2 (\phi_t + 2\phi_x)_t = [(1 - M^2)\phi_x + F\phi_x^2 + G\phi_y^2]_x + (\phi_y + H\phi_x\phi_y)_y + (\phi_z)_z \quad (1)$$

where the spatial coordinates x , y , and z are normalized by c_r ; the reference chord; and t is normalized by c_r/V . Here the time scale factor k of Ref. 7 is 1.0. The perturbation velocity potential ϕ is normalized by $c_r V$. The coefficients for the nonlinear terms in Eq. (1) can be defined as either^{19,20}

$$F = -\frac{1}{2}(\gamma + 1)M^2, G = \frac{1}{2}(\gamma - 3)M^2, H = -(\gamma - 1)M^2 \quad (2)$$

or

$$F = -\frac{1}{2}[3 - (2 - \gamma)M^2]M^2, G = -M^2/2, H = -M^2 \quad (3)$$

For $F = G = H = 0$ the linearized unsteady potential equation is obtained. The coefficients given by Eq. (2) are used for the calculations of this report for the RAE tailplane.

The boundary conditions imposed on the outer edges of the computational region in the original XTRAN3S were

$$\phi = 0 \quad \text{upstream}$$

$$\phi_x + \phi_t = 0 \quad \text{downstream}$$

$$\phi_z = 0 \quad \text{above and below}$$

$$\phi_y = 0 \quad \text{wing root}$$

$$\phi_y = 0 \quad \text{far spanwise}$$

$$[\phi_z] = [\phi_x + \phi_t] = 0 \quad \text{wake}$$

where $[]$ indicates jump in quantity across the wake here.

The wing flow tangency condition is

$$\phi_z^\pm = R_x^\pm + R_t^\pm; z = 0^\pm, x_{LE} < x < x_{TE}$$

where $R = r/c_r$.

The outer boundary conditions have recently been improved by Whitlow²¹ by implementing characteristic or "nonreflecting" boundary conditions. These revised conditions were in-

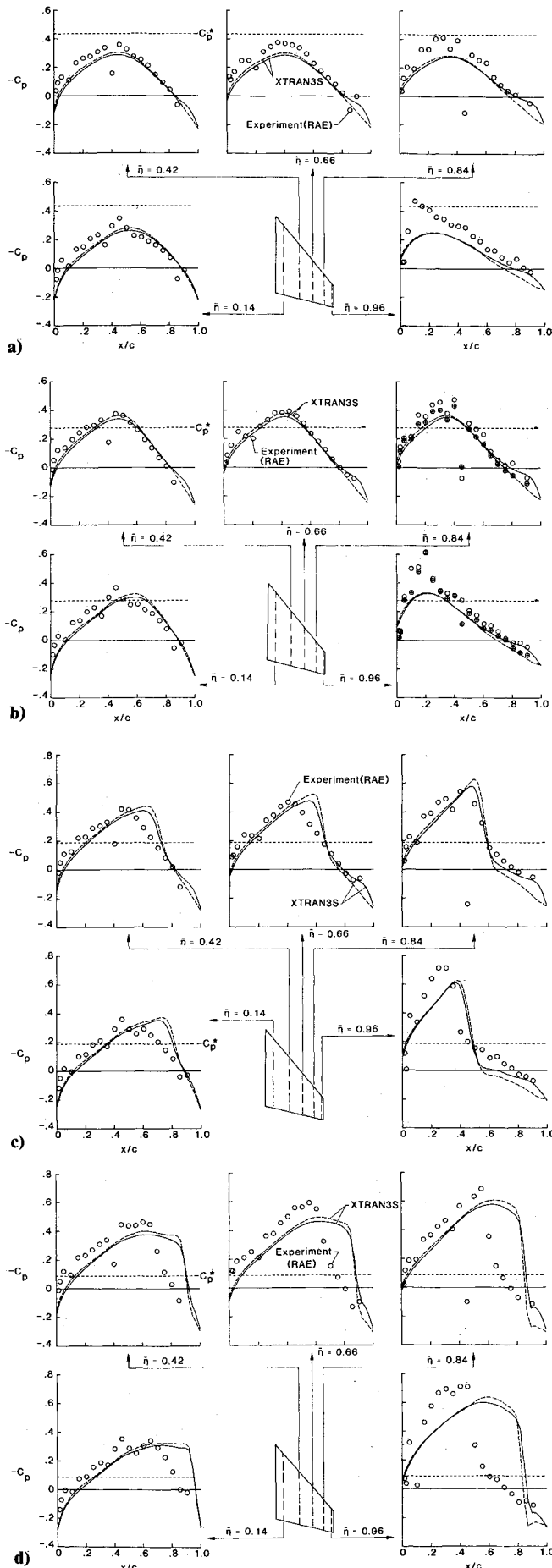


Fig. 4 Measured and calculated steady pressures for tailplane model.
a) $M=0.80$, b) $M=0.86$, c) $M=0.90$, d) $M=0.95$.

incorporated into the present version of the program used for the calculations for the RAE tailplane. The revised conditions are

$$\frac{1}{2} \left(\frac{2M^2}{B} + \frac{D}{\sqrt{B}} \right) \phi_t - \phi_x = 0 \quad \text{upstream}$$

$$\frac{1}{2} \left(-\frac{2M^2}{B} + \frac{D}{\sqrt{B}} \right) \phi_t + \phi_x = 0 \quad \text{downstream}$$

$$\frac{D}{2} \phi_t + \phi_z = 0 \quad \text{above}$$

$$\frac{D}{2} \phi_t - \phi_z = 0 \quad \text{below}$$

$$\phi_y = 0 \quad \text{wing root}$$

$$\frac{D}{2} \phi_t + \phi_y = 0 \quad \text{far spanwise}$$

where

$$B = 1 - M^2 + 2F\phi_x$$

$$D = 2M\sqrt{1 + 1/B}$$

Calculations have indicated that these characteristic boundary conditions significantly reduce the reflection of disturbances from the computational boundaries.²¹

Coordinate Transformation

The finite difference grid contains $60 \times 20 \times 40$ points in the x, y , and z directions for a total of 48,000 points. In physical space it conforms to the wing platform and the computational region is mapped to a rectangular domain using the shearing transformation

$$\xi = \xi(x, y), \quad \eta = y, \quad \zeta = z, \quad \text{and} \quad \tau = t$$

In computational space Eq. (1) becomes

$$\begin{aligned} M^2 \frac{\partial}{\partial \tau} \left[\frac{1}{\xi_x} \phi_\tau + 2\phi_\xi \right] &= \frac{\partial}{\partial \xi} \left[(1 - M^2) \xi_x \phi_\xi \right. \\ &+ F \xi_x^2 \phi_\xi^2 + G \xi_y^2 \phi_\xi^2 + 2G \xi_y \phi_\xi \phi_\eta \\ &+ G \phi_\eta^2 + \frac{\xi_y}{\xi_x} (\xi_y \phi_\xi + \phi_\eta) + H \xi_y \phi_\xi (\xi_y \phi_\xi + \phi_\eta) \Big] \\ &+ \frac{\partial}{\partial \eta} \left[\frac{1}{\xi_x} (\xi_y \phi_\xi + \phi_\eta) + H \phi_\xi (\xi_y \phi_\xi + \phi_\eta) \right] \\ &+ \frac{\partial}{\partial \zeta} \left[\frac{1}{\xi_x} \phi_\zeta \right] \end{aligned} \quad (4)$$

The original version of XTRAN3S used

$$\xi(x, y) = \frac{x - x_{LE}(y)}{c(y)} \quad (5)$$

to transform the streamwise coordinate. From Eq. (5), $\xi_x = 1/c(y)$, and ξ_y can be calculated analytically from Eq. (5) and the equations describing the wing planform. Using Eq. (5) results in a physical region whose streamwise extent is proportional to the local chord at each span station and, for highly swept and tapered wings, results in a highly skewed mesh in

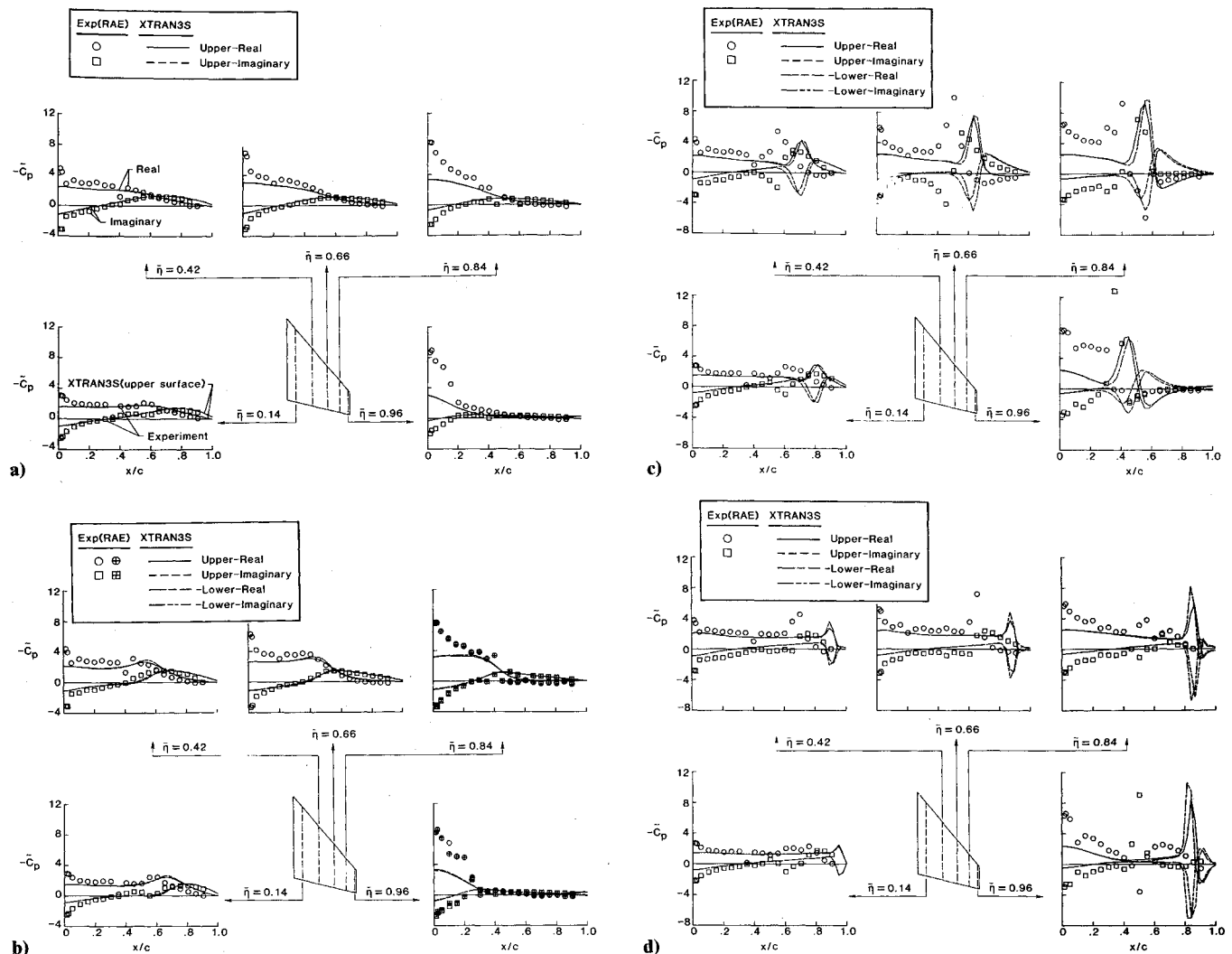


Fig. 5 Measured and calculated unsteady pressure distributions for tailplane model oscillating at approximately 70 Hz. a) $M=0.80$, $k=0.490$; b) $M=0.86$, $k=0.456$; c) $M=0.90$, $k=0.441$; d) $M=0.95$, $k=0.420$.

the far field of the physical domain. The resulting skewness of the grid led to numerical instabilities that restricted the application of XTRAN3S to wings of low sweep and low taper. The grid has been revised such that in the physical domain, the computational region is a rectangular box, thus alleviating the skewness of the grid.

Versions of this type of grid arrangement have been given previously.^{14,15} In Ref. 15, a smooth stretching was used to map the regions from the wing to the upstream or downstream boundaries. Good results were obtained for the F-5 wing which is highly swept and highly tapered. In Ref. 14, Eq. (5) is retained on the wing and similar equations are used in the upstream and downstream regions with $c(y)$ replaced by the local distance from the wing to the boundary of the region. Such a technique permits analytical evaluation of ξ_x and ξ_y , but results in discontinuous values of these quantities at the leading and trailing edges. Good results have also been obtained for the F-5 wing by that method.¹⁴

Herein a finite-difference grid is used that is similar to that of Ref. 15. In the physical domain the grid is described analytically to give a smoothly varying mesh spacing. The ξ -distribution of points (for all values of η) in the ξ - η domain is chosen to be the same as the x distribution of points along the root chord in the physical domain. The values of ξ_x and ξ_y are calculated numerically using second-order finite-difference formulas at each point in the computational domain since an analytical relationship between ξ and x is not available.

Finite-Difference Grid

The grid used for the computations presented in this report is shown in Fig. 2 along with the wing planform. The grid is defined in the following manner. First, Eq. (5) is used on the wing planform. The x spacing of points along the chord essentially is that developed earlier^{12,22} with 39 points along the local chord; 38 points are equispaced from $x/c = 1/38$ to 1.0, and an additional point is located at $x/c = 1/(3 \times 38)$. The grid extends from 20 wing root chords upstream of the wing root leading edge to 20 chord downstream of the wing root trailing edge. Eleven grid lines are used ahead of the wing and ten aft. The wing leading edge is centered between grid lines.

The spacing ahead of the wing in the physical domain at each spanwise location is given by an equation that is cubic in the index of the grid point running from the leading edge to the upstream boundary. The coefficients of the cubic are determined from the location of the leading edge, the location of the upstream boundary, the symmetry of the points ahead and aft of the leading edge, and by setting the second derivative to zero at leading edge. The equations are detailed in Ref. 13. The spacing of the grid points downstream is also given by a cubic equation determined in a similar manner.

Fourteen rows of points are used along the wing (including the points inboard of and on the plane of symmetry). The rows are distributed along the span using a cosine distribution with 13 grid rows on the wing. The first spanwise station is at 12% span and the last one at 99.3% span. This distribution of

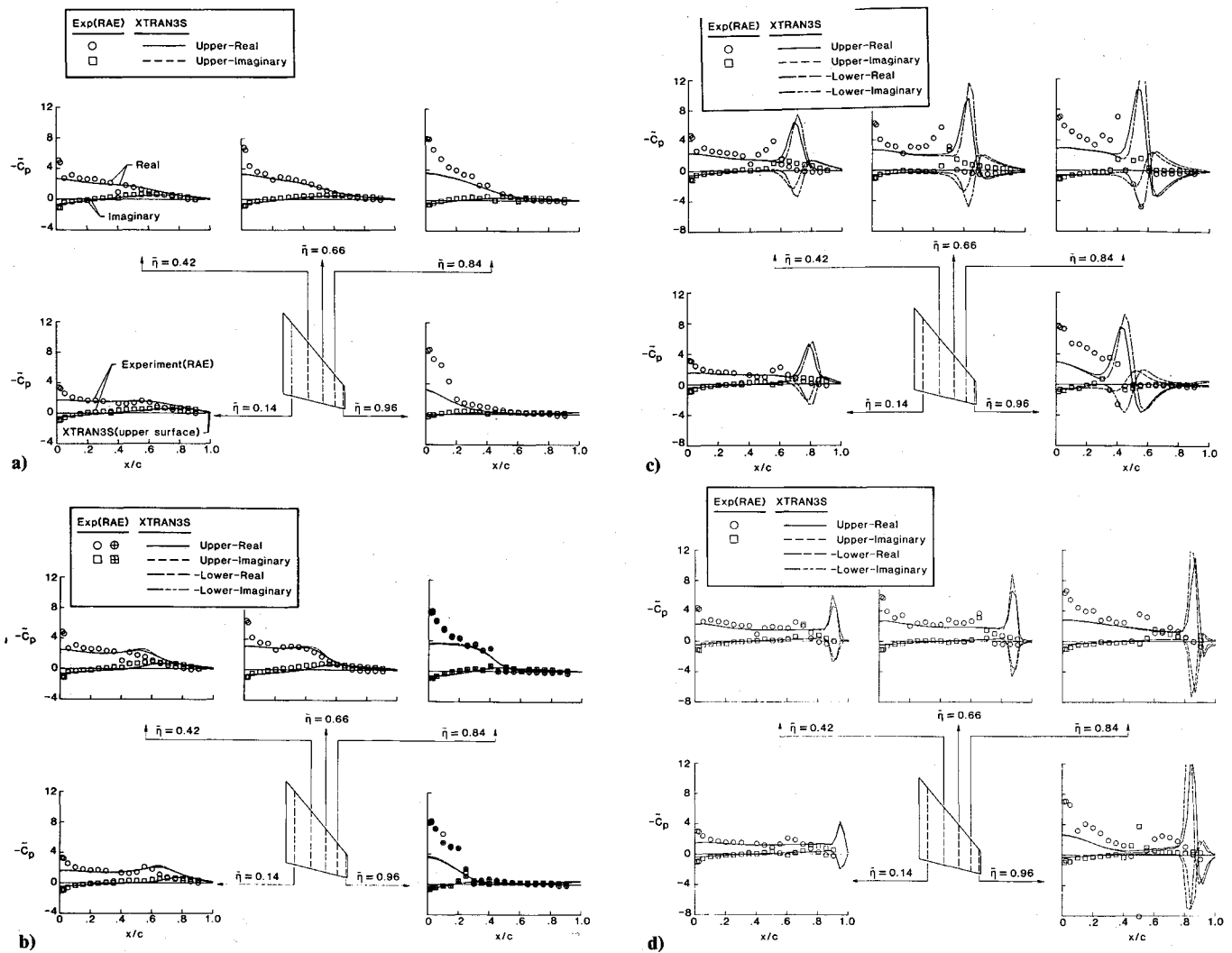


Fig. 6 Measured and calculated unsteady pressure distributions for tailplane oscillating at approximately 33 Hz. a) $M = 0.80$, $k = 0.234$; b) $M = 0.86$, $k = 0.222$; c) $M = 0.90$, $k = 0.221$; d) $M = 0.95$, $k = 0.201$.

grid points is used to emphasize the definition of loads in the tip region which are critical for aeroelastic analysis.

Outboard of the tip, the wing planform is extended smoothly to the far spanwise boundary at 1.5 spans. The mid-chord line of the wing is extended to the far spanwise boundary as a parabola that has a slope of the wing midchord at the tip and is perpendicular to the far boundary. The wing leading and trailing edges are extended using cubic equations that match leading and trailing edge slopes and intersect the far spanwise boundary perpendicularly at one half the tip chord fore and aft of the midchord extension. The same streamwise distribution of points that is used on the wing is used in the outboard region.

The η -distribution of points in the outboard region also is given by a cubic equation. The cubic is determined in a manner similar to the equation upstream of the wing. The first row of points outboard of the wing and the last row on the wing are located symmetrically about the tip.

In previous versions of XTRAN3S, points inboard of the wing root were located by extrapolating the first outboard points through the wing root using straight lines. For the calculations for this wing the x coordinates of the points located inboard of the plane of symmetry are reflected as mirror images of the points at the first station outboard of the plane of symmetry. The values of ξ_x and ξ_y are then calculated by the same finite difference equations as previously indicated. This grid variation, first implemented by Dr. John T. Batina of Langley Research Center, has been shown to improve the pressures calculated along the centerline. Further improvement has been obtained by Batina by slightly round-

ing the wing apex. This change was not implemented in the version of XTRAN3S used here.

The grid extends 25 root chords above and below the wing. Twenty rows of points are used above, and 20 rows are used symmetrically below the wing. The distribution of points is that previously developed and applied.^{14,21}

The resulting grid is smooth and embeds the planform smoothly. This grid appears to be reasonable, but since to date only limited variations have been investigated for three-dimensional configurations, the grid cannot be considered an optimal choice. The grid is reasonably fine on the wing but is relatively coarse off the wing.

Results and Discussion

RAE AGARD Tailplane Model

Calculations have been made with XTRAN3S for the RAE tailplane near zero angle of attack and for Mach numbers of 0.80, 0.86, 0.90, and 0.95. The numerical algorithm used in XTRAN3S is an alternating-direction implicit scheme but with some terms treated explicitly. Treating some terms explicitly leads to a CFL (Courant-Friedrichs-Lewy) type of stability restriction in the time accurate finite difference solution. For the calculations for the tailplane model, this stability limit was found to be near $\Delta t = 0.0075$. This small time step results in a large number of steps per cycle which increases with decreasing frequency. Calculations were made only for frequencies of 33 and 70 Hz which required approximately 2000 and 1000 time steps per cycle, respectively. Generally three cycles of oscillation were calculated starting from a converged steady

flow solution. The last cycle was analyzed for the Fourier components. For the steady calculations the program was run in a time asymptotic manner for 1500 time steps to assure convergence. On the VPS32, XTRAN3S requires approximately 1.5 s of CPU time per time step. The code is not vectorized except for that generated by the compiler.

The measured airfoil ordinates have been used to define the wing surface slopes required for input to XTRAN3S. The measured ordinates were fitted with a parametric spline with smoothing,²³ and the slopes were calculated from the spline fit.

The experimental data points presented herein were obtained from a digital tape supplied by the RAE and are presented unedited in the figures.

Results for Steady Pressures

The variation of the calculated static pressure with Mach number is shown in Fig. 3. The pressures for the upper surface ($-C_p$) are shown for an angle of attack of -0.3 deg. Typical of highly swept wings, the leading edge pressures change from compression at the root to expansion at the tip. The pressures are supercritical at $M=0.86$, and at $M=0.90$, a strong shock wave is formed which is particularly pronounced near the tip. At $M=0.95$, the strong shock has moved rearward to near the trailing edge.

The calculated and measured pressures are compared in Figs. 4a–4d. Points for repeated measurements are shown with plus signs within the symbols. The experimental data for this wing with a nominally symmetric airfoil section indicated that zero bending moment was obtained near an angle of attack of 0.3 – 0.4 deg indicating a small amount from tunnel flow angularity. The results herein (both steady and unsteady) were run at 0.3 deg angle of attack, which is near the experimental estimate.

For $M=0.80$ the agreement is reasonable for the inboard stations (Fig. 4a). However, the agreement deteriorates at the outboard stations. The pressure expansion over the forward portion of the airfoil is generally underpredicted. Similar trends are noted also for $M=0.86$ but with improved agreement inboard (Figs. 4a and 4b). There is a strong peak in the measured pressures near the tip leading edge for these two Mach numbers which may indicate a viscous effect around the sharply cut-off tip. For $M=0.90$ (Fig. 4c) there is a shock which is particularly strong near the tip and whose strength is overpredicted by XTRAN3S. Again the agreement on the forward portion of the airfoil is reasonable and underpredicted by XTRAN3S. At $M=0.95$ (Fig. 4d), the shock location is predicted to be significantly rearward of the experimental location.

Overall, XTRAN3S predicts the general trends in the static pressures fairly well, but with poor agreement near the tip. Best agreement is obtained near critical freestream Mach number. An underprediction of the expansion pressures is indicated with an overprediction of the strength of transonic shock waves. One limitation of TSP theory as implemented in XTRAN3S is that only the streamwise velocities are considered in the expressions for pressure. For highly swept wings, spanwise flow effects may need to be considered, especially for nonzero angles of attack.

Unsteady Pressures

The comparison of calculated and measured unsteady pressures for the 70-Hz cases for each of the Mach numbers is shown in Figs. 5a–5d. The data are presented along each chord in the form of real and imaginary components of the first harmonic of the unsteady pressure. For $M=0.80$ the calculated results are shown only for the upper surface; the results for the lower surface were identical. For the higher Mach numbers, the lower surface pressure are shown with their sign changed. Only small differences are shown in the calculated upper and lower surface pressures for $M=0.86$, with modest differences shown in the region of the shock at $M=0.90$ and $M=0.95$.

For $M=0.80$ and 0.86 there is good agreement between calculated and measured trends, and good quantitative agreement of the pressures over the inboard sections where the agreement for the pressure results was good. As might be anticipated, the overall agreement at the tip is not good where the steady results were not very good. In addition, the XTRAN3S results do not show the sharp pressure peak near the leading edge that is shown by the experimental results. A calculation for the $M=0.86$ case has been made using the Euler equations (Ref. 24). Although no detailed comparisons have been made, the trends are comparable, but with somewhat better agreement near the leading edge.

For $M=0.90$ and 0.95 and 70 Hz, the agreement in trends and magnitudes on the forward portion of the airfoil is comparable to that at the lower Mach numbers. However, near the shock, the calculated results deviate significantly from the measured values. The unsteady results are seriously affected by the differences in steady flow shock location and strength.

Where repeat points are shown, the agreement of the two measurements is very good (Fig 5b, for example) and the symbols with and without plus signs almost overlay.

The comparison of calculated and measured results for the 33-Hz cases is shown in Figs. 6a–6d. For 33 Hz, the value of k varies from 0.234 at $M=0.80$ to 0.201 at $M=0.95$. Comparison of the 33- and 70-Hz data shows about the same trends and magnitudes with the imaginary part for 33 Hz being about one-half of that for 70 Hz as expected. The level of agreement is also comparable to the higher-frequency results but with better agreement for the imaginary parts. For $M=0.90$ and 0.95 the calculated peaks near the shock are larger than for the higher-frequency cases. Such peaks are not observed on the experimental data.

Several cases have been calculated for the F-5 planform using XTRAN3S.^{14,15} The agreement with the experimental data is better than for the RAE tailplane. However, the calculated shock wave strength is also overpredicted for the F-5 for $M=0.95$. The F-5 wing is significantly thinner as it has a slightly cambered 4.8% thick section and should be more consistent with TSP theory. Applications of XTRAN3S to the calculation of pressures on thick supercritical wings have also been given.^{10,12,14,17} Generally the correlation of calculated and experimental results is less satisfactory than for the F-5 or the tailplane configurations. Improvements in the theory or further development of the code may overcome some of these current limitations. It should also be noted that significant questions have been raised concerning the accuracy of isentropic potential theory²⁵ for two-dimensional flows. A nonisentropic small disturbance theory has recently been developed to alleviate some of these problems in both the two-dimensional⁵ and the three-dimensional²⁶ cases.

Concluding Remarks

An overview of the transonic small perturbation code XTRAN3S and a recently developed finite-difference grid have been given. Data measured by the British RAE for the AGARD SMP tailplane have been compared with results calculated using XTRAN3S. Several steady and higher frequency unsteady cases with near zero angle of attack and for subsonic and transonic Mach numbers are presented.

Good overall trends were obtained with XTRAN3S for the RAE tailplane model but poor agreement was found near the tip, the leading edge, and for strong shock waves. Extensive computer resources are required to run XTRAN3S for an investigation of this type. Further effort is needed to reduce the resources required by increasing the numerical stability to permit large time steps. Further development is needed to treat thick supercritical wings with shock waves.

References

- 1 Edwards, J. W., Bland, S. R., and Seidel, D. A., "Experience with Transonic Unsteady Aerodynamics Calculations," Transonic

Unsteady Aerodynamics and its Aeroelastic Applications, AGARD CP 374, Jan. 1985, Paper 5.

²Goorjian, P. M. and Guruswamy, G. P., "Unsteady Transonic Aerodynamic and Aeroelastic Calculations About Airfoils and Wings," *Transonic Unsteady Aerodynamics and its Aeroelastic Applications*, AGARD CP 374, Jan. 1985, Paper 14.

³Howlett, J. T., "Effective Self-Consistent Viscous-Inviscid Solutions for Unsteady Transonic Flow," AIAA Paper No. 85-0482, Jan. 1985.

⁴Guruswamy, P. and Goorjian, P. M., "Effects of Viscosity on Transonic-Aerodynamic and Aeroelastic Characteristics of Oscillating Airfoils," *Journal of Aircraft*, Vol. 21, Sept. 1984, pp. 700-707.

⁵Fuglsang, D. F. and Williams, M. H., "Non-Isentropic Unsteady Transonic Small Disturbance Theory," AIAA Paper 85-0600, April 1985.

⁶Batina, J. T., "Unsteady Transonic Flow Calculations for Two-Dimensional Canard-Wing Configurations with Aeroelastic Applications," AIAA Paper 85-0585, April 1985.

⁷Borland, C. J. and Rizzetta, D. P., *Transonic Unsteady Aerodynamics for Aeroelastic Applications—Vol. I: Technical Development Summary*, AFWAL TR 80-3107, Vol. I, June 1982.

⁸Hess, R. W., Wynne, E. C., and Cazier, F. W., Jr., "Static and Unsteady Pressure Measurements on a 50 Degree Clipped Delta Wing at $M=0.9$," NASA TM 83297, April 1982.

⁹Sandford, M. C., Ricketts, R. H., Cazier, F. W., Jr., and Cunningham, H. J., "Transonic Unsteady Airloads on an Energy Efficient Transport Wing with Oscillating Control Surfaces," *Journal of Aircraft*, Vol. 18, July 1981, pp. 557-561.

¹⁰Ricketts, R. H., Sandford, M. C., Seidel, D. A., and Watson, J. J., "Transonic Pressure Distributions on a Rectangular Supercritical Wing Oscillating in Pitch," *Journal of Aircraft*, Vol. 21, Aug. 1984, pp. 576-582.

¹¹Seidel, D. A., Sandford, M. C., and Eckstrom, C. V., "Measured Unsteady Transonic Aerodynamic Characteristics of an Elastic Supercritical Wing with an Oscillating Control Surface," AIAA Paper 85-0598-CP, April 1985.

¹²Seidel, D. A., Bennett, R. M., and Ricketts, R. H., "Some Recent Applications of XTRAN3S," AIAA Paper 83-1811, July 1983.

¹³Bennett, R. M., Seidel, D. A., and Sandford, M. C., "Transonic Calculations for a Flexible Supercritical Wing and Comparison with Experiment," AIAA Paper 85-0665, Apr. 1985.

¹⁴Borland, C. J. and Sotomayer, W. A., "An Algorithm for Unsteady Transonic Flow About Tapered Wings," AIAA Paper 84-1567, June 1984.

¹⁵Guruswamy, P. G. and Goorjian, P. M., "An Efficient Algorithm for Unsteady Transonic Aerodynamics of Low Aspect Ratio Wings," *Journal of Aircraft*, Vol. 22, March 1985, pp. 193-199.

¹⁶Tijedeman, H. et al., "Transonic Wind Tunnel Tests on an Oscillating Wing with External Store," AFFDL-TR-78-194, Parts I & II, Dec. 1978.

¹⁷Ruo, S. Y., Malone, J. B., Horsten, J. J., and Houwink, R., "The LANN Program: An Experimental and Theoretical Study of Steady and Unsteady Transonic Airloads on a Supercritical Wing," AIAA Paper 83-1686, July 1983.

¹⁸Mabey, D. G., Welsh, B. L., and Cripps, B. E., "Measurements of Steady and Oscillatory Pressures on a Low Aspect Ratio Model at Subsonic and Supersonic Speeds," British RAE Technical Rept. 84095, Sept. 1984.

¹⁹Lomax, H., Bailey, F. R., and Ballhaus, W. F., "On the Numerical Simulation of Three-Dimensional Transonic Flow with Application to the C-141 Wing," NASA TN D-6933, Aug. 1973.

²⁰Van der Vooren, J., Sloof, J. W., Huizing, G. H., and van Essen, A., "Remarks on the Suitability of Various Transonic Small Perturbation Equations to Describe Three-Dimensional Transonic Flow, Examples of Computations Using a Fully-Conservative Rotated Difference Scheme," *Symposium Transonicum II, Goettingen, West Germany, September 1975, Proceedings*, Springer-Verlag, Berlin, 1976, pp. 557-566.

²¹Whitlow, W., Jr., "Characteristic Boundary Conditions for Three Dimensional Transonic Unsteady Aerodynamics," NASA TM 86292, Oct. 1984.

²²Seidel, D. A., Bennett, R. M., and Whitlow, W., Jr., "An Exploratory Study of Finite-Difference Grids for Transonic Unsteady Aerodynamics," AIAA Paper 83-0503, Jan. 1983, see also NASA TM 84583, Dec. 1982.

²³Desmarais, R. N. and Bennett, R. M., "Computer Programs for Plotting Curves with Various Dashed-Line Sequences," NASA TM 2465, Feb. 1972.

²⁴Salmond, D. J., "Calculation of Harmonic Aerodynamic Forces on Aerofoils and Wings From Euler Equations," Paper 6 in "Transonic Unsteady Aerodynamics and its Aeroelastic Applications," AGARD 374, Jan. 1985.

²⁵Salas, M. D. and Gumbert, C. R., "Breakdown of the Conservative Potential Equation," AIAA Paper 85-0367, Jan. 1985.

²⁶Gibbons, M. D., Whitlow, W., Jr., and Williams, M. H., "Nonisentropic Unsteady Three Dimensional Small Disturbance Potential Theory," AIAA Paper 86-0863, May 1986.